





Article

Overview of PM₁₀, PM_{2.5} and BC and Their Dependent Relationships with Meteorological Variables in an Urban Area in Northwestern Morocco

Youssef Bounakhla ^{1,†} , Abdelfettah Benchrif ^{2,*,†} , Francesca Costabile ³ , Mounia Tahri ² , Bassma El Gouch ⁴, El Kafssaoui El Hassan ¹, Fatiha Zahry ² and Moussa Bounakhla ²

¹ Faculty of Sciences, Ibn Tofail University, Kenitra 14000, Morocco

² National Centre for Nuclear Energy, Science and Technology (CNESTEN), Rabat 10000, Morocco

³ Institute for Atmospheric Sciences and Climate, National Research Council, 00133 Rome, Italy

⁴ Faculty of Sciences and Technologies, Sidi Mohamed Ben Abdellah University, Fes 30000, Morocco

* Correspondence: abenchrif@gmail.com or benchrif@cnesten.org.ma

† These authors contributed equally to this work.

Abstract: At an urban site in Kenitra, Morocco, two aerosol size fractions (PM_{2.5} and PM₁₀) were sampled for four seasons to characterize the seasonal trends of particulate (PM) and carbonaceous (BC) aerosols. An in-depth statistical analysis of the lag-effects of meteorology on collected data was investigated using uni- and multivariate linear regression analyses. The results revealed significant seasonal trends for PM₁₀, PM_{2.5}, and BC. PM concentrations showed the maximum values in autumn ($61.4 \pm 24.5 \mu\text{g}/\text{m}^3$ for PM₁₀ and $21.2 \pm 8.2 \mu\text{g}/\text{m}^3$ for PM_{2.5}), while the minimum was observed in winter ($40.2 \pm 17.1 \mu\text{g}/\text{m}^3$) for PM₁₀ and in summer ($14.3 \pm 3.3 \mu\text{g}/\text{m}^3$) for PM_{2.5}. High BC concentrations were recorded in summer ($6.3 \pm 4.2 \mu\text{g}/\text{m}^3$, on average). The relative humidity 1–2 days earlier showed a higher negative correlation with the PM concentrations (except in winter), and the temperature 1–3 days earlier showed a negative correlation with the PM_{2.5} in winter and summer and a positive one with the PM₁₀ in autumn. Wind speed was negatively associated with PM₁₀ on the current day in winter and 3 days earlier in summer. However, diverse effects of wind speed on PM_{2.5} were observed (negative in summer and positive in spring). These results confirm the important role of meteorology in the formation of urban air pollution with pronounced variations in different seasons.

Keywords: urban aerosols; PM₁₀; PM_{2.5}; black carbon; meteorological variables; multivariate linear regression; CWT; Northwestern Morocco



Citation: Bounakhla, Y.; Benchrif, A.; Costabile, F.; Tahri, M.; El Gouch, B.; El Hassan, E.K.; Zahry, F.; Bounakhla, M. Overview of PM₁₀, PM_{2.5} and BC and Their Dependent Relationships with Meteorological Variables in an Urban Area in Northwestern Morocco. *Atmosphere* **2023**, *14*, 162. <https://doi.org/10.3390/atmos14010162>

Academic Editor: Griša Močnik

Received: 24 November 2022

Revised: 9 January 2023

Accepted: 10 January 2023

Published: 12 January 2023



Copyright: © 2023 by the authors. Licensee MDPI, Basel, Switzerland. This article is an open access article distributed under the terms and conditions of the Creative Commons Attribution (CC BY) license (<https://creativecommons.org/licenses/by/4.0/>).

1. Introduction

Urban air pollution has become a global problem due to its negative impact on human health and the environment. The issue of urban pollution is rapidly gaining importance in modern societies, where the relationship between environmental conditions and health is one of the main issues. Particulate matter (PM), including PM₁₀ (aerosols diameters from 2.5 to 10 μm) and PM_{2.5} (aerosols < 2.5 μm in diameter), occupies an important place in this discussion, and numerous disciplines (from chemistry to epidemiology) have produced research in this area [1,2]. In the case of the large fraction of atmospheric particulate matter in many urban areas, carbonaceous aerosols play a significant role in air pollution, visibility, health, and climate impacts [3,4]. Organic carbon (OC) and the primary pollutant black carbon (BC) (sometimes referred to as elemental carbon (EC)) are emitted from anthropogenic combustion sources. They are mainly generated through three processes: wood burning, fossil fuel burning, and biogenic emissions [5]. Several investigations have addressed the specifics of BC mass concentration in different parts of Morocco. For example, in northern Morocco, Benchrif et al. [6] reported that the BC makes up 18% to 22% of the

fine aerosol mass, and OC ranges from 30 to 38% in terms of aerosol loading regions. They emphasized that a low OC/EC ratio (1.7–1.9) indicates that carbonaceous aerosols are emitted locally by traffic rather than transported over long ranges. In our previous studies, we found that fossil fuel combustion is the most significant contributor to BC in Kenitra, Morocco [5], and Salé, Morocco [7], with an average BC mass concentration of $0.90 \mu\text{g}/\text{m}^3$ and $1.9 \mu\text{g}/\text{m}^3$, respectively.

To provide crucial information about the formation process and the effects of particle origin, $\text{PM}_{2.5}$ to PM_{10} ratios are commonly used. These ratios are considered a useful indicator of the type of dominant pollutant in a given area [8] and are used to analyze the origin of PM pollution, whether anthropogenic-related or not [9]. For instance, a low $\text{PM}_{2.5}/\text{PM}_{10}$ ratio indicates a higher contribution to PM_{10} targeting a significant contribution from natural aerosols through natural processes. Conversely, a higher $\text{PM}_{2.5}/\text{PM}_{10}$ ratio is the result of lower PM_{10} concentrations and a higher contribution from finer anthropogenic aerosols [10,11]. In addition, Wang et al. [12] demonstrated that the distributions of $\text{PM}_{2.5}/\text{PM}_{10}$ ratios are seasonal and spatially dependent. Regarding carbonaceous aerosol compounds, Gidhagen et al. [13] emphasized that BC to $\text{PM}_{2.5}$ ratios may provide speciation of $\text{PM}_{2.5}$, which varies depending on the combustion process (e.g., residential wood combustion), the fuel type (e.g., gasoline, natural gas), and the application (e.g., use of natural gas for power generation). Ntziachristos and Samaras [14] suggested that BC/ $\text{PM}_{2.5}$ ratios, in addition to organic matter (OM) to black carbon (OM/BC) ratios, can be applied to the exhaust PM emissions for different vehicle technologies. For instance, BC/ $\text{PM}_{2.5}$ ratios are reported by previous studies conducted in a rural area of Tongyu, China, to be 0.8% [15]; in an urban (near jogging trails) in Macau, China, ranging from 1.6 to 44.8% [16]; in an urban (near roadways) area of Beijing, China, between 2.1 and 5.4% [17]. Furthermore, the high correlation between $\text{PM}_{2.5}$ and BC advocates that they share common regional sources, such as winter biomass burning in Beijing [17,18]. Yu et al. [17] reported that $\text{PM}_{2.5}$ and BC had comparable atmospheric lifetimes, in the order of weeks, making their concentrations similarly affected by air movements such as convection (atmospheric stability) and advection (wind), especially when regional sources are dominant.

Many studies on air pollution from particulate matter have been conducted in various locations in Africa over the last decade. For example, in Ashaiman, Ghana, Dotse et al. [19] found an average of $96.6 \mu\text{g}/\text{m}^3$, $23.3 \mu\text{g}/\text{m}^3$, and $4.9 \mu\text{g}/\text{m}^3$ in PM_{10} , $\text{PM}_{2.5}$, and BC from February to May 2008, respectively. In Dar-es-Salaam, Tanzania, between August and September 2005, Mkoma et al. [20] found an average of $76 \pm 32 \mu\text{g}/\text{m}^3$, $26 \pm 7 \mu\text{g}/\text{m}^3$, and $3.6 \pm 1.3 \mu\text{g}/\text{m}^3$ in PM_{10} , $\text{PM}_{2.5}$, and BC, respectively; and $52 \pm 27 \mu\text{g}/\text{m}^3$, $19 \pm 10 \mu\text{g}/\text{m}^3$, and $4.0 \pm 2.3 \mu\text{g}/\text{m}^3$ in the period between April and May 2006. In Morocco, namely in the city of Kenitra, previous studies [21] recorded an average concentration of $161.1 \mu\text{g}/\text{m}^3$ and $50.7 \mu\text{g}/\text{m}^3$ for PM_{10} and $\text{PM}_{2.5}$ from May 2007 to May 2008. However, to the best of the author's knowledge, BC concentrations have never been documented in Kenitra.

This study aims to evaluate the characteristics of, effects of meteorological parameters on, and the temporal variations in aerosol mass concentrations (PM_{10} , $\text{PM}_{2.5}$, and BC) as measured in four different seasons at an urban site in Kenitra city. Kenitra is characterized by high temperature in summer (mid-August to September) and low in winter (January to mid-February). It is usually windy and known for high relative humidity (>70%). This comprehensive study attempts to provide necessary answers to the following questions: (i) What are the temporal changes in PM_{10} , $\text{PM}_{2.5}$, and BC values at a seasonal scale? (ii) How are the critical pollutants characterized in comparison to African and worldwide locations? (iii) Is the univariate correlation approach sufficient to investigate the effect of meteorological variables on temporal variations and trends in air pollutant levels? (iv) Do the long-range transported aerosols and local activities have an impact on PM_{10} , $\text{PM}_{2.5}$, and BC levels in Kenitra?

2. Materials and Methods

2.1. Instrumentation and Sampling

Fine $PM_{2.5}$ (aerosols $< 2.5 \mu\text{m}$ in diameter) and coarse $PM_{2.5-10}$ (aerosols diameters from 2.5 to $10 \mu\text{m}$) measurements were performed from July 2020 to April 2021 in Kenitra (Figure 1) in an urban residential area (Lat: 34.234194 ; Lon: -6.614889). They were collected on 37-mm diameter Nuclepore track-etched polycarbonate filters (Whatman Inc., Middlesex, UK) using the Dichotomous Sampler (Model 241, Graseby Andersen, Fulton, GA, USA). The sampler consists of an omnidirectional aerosol inlet, a virtual impactor assembly, two 37-mm diameter filter holders, and a tripod mount. It samples simultaneously fine and coarse aerosol fractions on separate filters. Two filters ($PM_{2.5}$ and $PM_{2.5-10}$) were collected for each day of sampling. The sampler operated at $1 \text{ m}^3/\text{h}$ for a sampling period of 24 h.

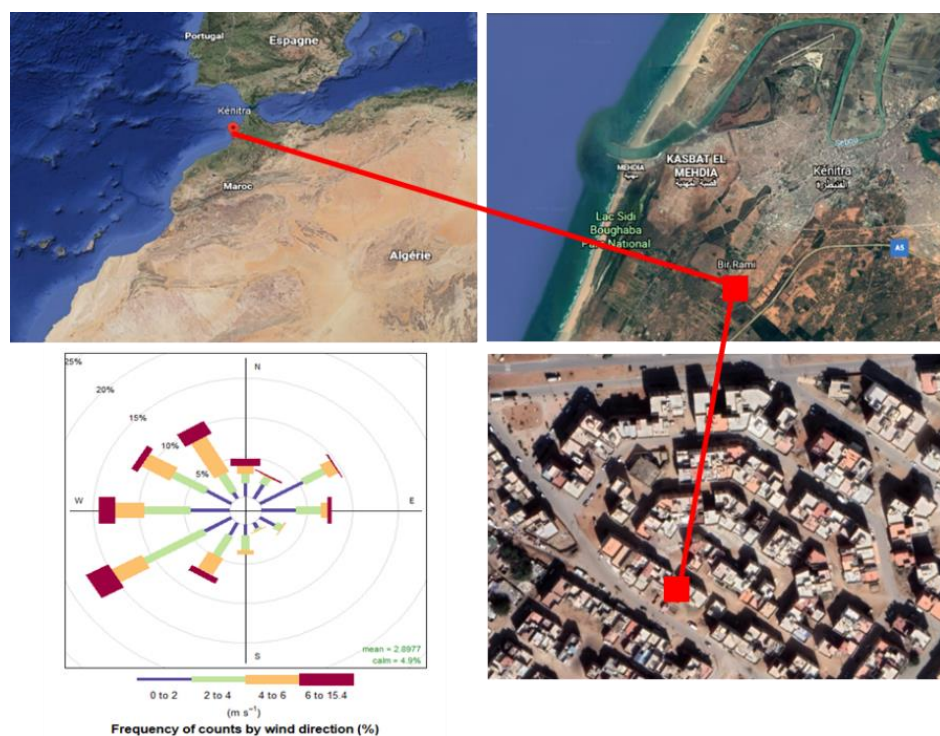


Figure 1. The sampling site (red square) is located in the Atlantic region (upper left panel), at a distance from the city center (upper right panel), and in an urban area (bottom right panel). The wind was based on hourly averages of wind speed and wind direction (bottom left panel).

The filters from the dichotomous sampler were weighed before and after sampling, using a Sartorius microbalance (ME5, Göttingen, Germany) with $1 \mu\text{g}$ sensitivity. After 24 h of equilibrium at room temperature with the requisite ambient relative humidity, filter weighing was achieved. The error for each weighing was generally in the order of $18 \mu\text{g}$, corresponding to an average uncertainty of 9% for $PM_{2.5}$ and 6% for $PM_{2.5-10}$ measurements. Loaded filters were handled equally before being weighed for the gravimetric determination of PM mass. The PM_{10} mass concentrations were calculated by the arithmetic sum of the $PM_{2.5-10}$ and the corresponding $PM_{2.5}$ mass concentrations.

A multi-wavelength absorption black carbon instrument (MABI) measures light absorption in a filter at seven different wavelengths: 405 nm, 465 nm, 525 nm, 639 nm, 870 nm, 940 nm, and 1050 nm [22] and is also used to differentiate between light-absorbing carbon from high-temperature fossil fuel combustion (such as diesel vehicle engines) and biomass burning. MABI provides a powerful tool for identifying source contributions and determining the light-absorbing carbon content of filters using quantitative analysis [23].

2.2. Meteorological Data

The meteorological observations were retrieved from NOAA Integrated Surface Database (ISD) meteorological data [24]. Meteorological data are local measurements recorded at the weather station of Kenitra Airport (34.274° N, 6.569° W), about 6.3 km from our study site. The 6 h meteorological data includes wind speed (WS), wind direction (WD), relative humidity (RH), air pressure (P), and air temperature (T). The R package *worldmet* [25] was used for accessing the ISD database (<https://www.ncdc.noaa.gov/isd>; accessed on 1 March 2022).

2.3. Geographical Origins

To analyze the transport pathways and potential source areas of PM₁₀, PM_{2.5}, and BC in Kenitra, backward trajectory analysis and concentration-weighted trajectory (CWT) modelling was performed. Combining atmospheric concentrations measured at the receptor site with air mass back trajectories and residence time information, the CWT model helps to geographically assess the air mass pathways responsible for high concentrations [26]. For this purpose, hourly 48 h back trajectories calculated every 6 h (0, 6, 12, and 18 h) and arriving at 500 m above ground level were computed from the PC-based version of HYSPLIT version 5.0 [27,28]. CWT calculations were performed using the ZeFir Igor package [29].

2.4. Multivariate Linear Regression Analysis

Multivariate linear regression (MLR) analysis was performed to estimate the extent of variation of each studied pollutant, taking into account the meteorological impact. It is often used to model the relationship between pollutant concentration (as a response variable) and meteorological parameters (as independent variables). MLR uses the least-squares technique to estimate the regression coefficients (r^2) between actual and predicted values. The level of each pollutant is modelled by the following linear regression, given in Equation (1):

$$\text{Pollutant } (\mu\text{g}/\text{m}^3) = b_1X + b_2X^2 + b_3X^3 + C \quad (1)$$

where the Pollutant is the response variable; b_i represents the regression coefficients measuring the effect of the corresponding meteorological variable on the level of the Pollutant; X^i represents the independent variables; C is the intercept of the model.

While most previous studies that used the MLR model [30,31] assessed the line of best fit that minimizes the variances of each of the included variables with respect to the dependent variable, in this study the comprehensive evaluation of the data collected, including daily collected PM₁₀, PM_{2.5}, and BC concentrations, is based on the following steps: (1) before the modeling process, visualizing the correlation matrix and highlighting the most strongly correlated variables; (2) because data often contains irregularities, applying the regression model results in a predictive model that is far from optimal. The detection and exclusion of outliers are then performed using visualization methods, notably the `ols_plot_resid_lev()` function from the `olsrr` R package [32]; (3) evaluation and selection of the best linear regression model by applying the Akaike information criterion (AIC) [33], the Bayesian information criterion (BIC) [34,35], and the Mallowss-C_p (C_p) [36]. All of these are unbiased criteria for estimating the prediction error of the Mean Square Error (MSE) model. The lower these criteria values, the better the model. The flowchart detailing the actual processing steps followed in this study is shown in Figure 2.

The data for each meteorological parameter has been divided into two specific subsets: The training data, accounting for 80% of the total data, and the test data, at 20%. For validation, the cross-validation (CV) approach was used to estimate the accuracy of the generated model. The best-fitting models are characterized by a large value of the coefficient of determination (r^2) and a low mean square error (RMSE), and a small difference between the RMSE of the training set and the test set.

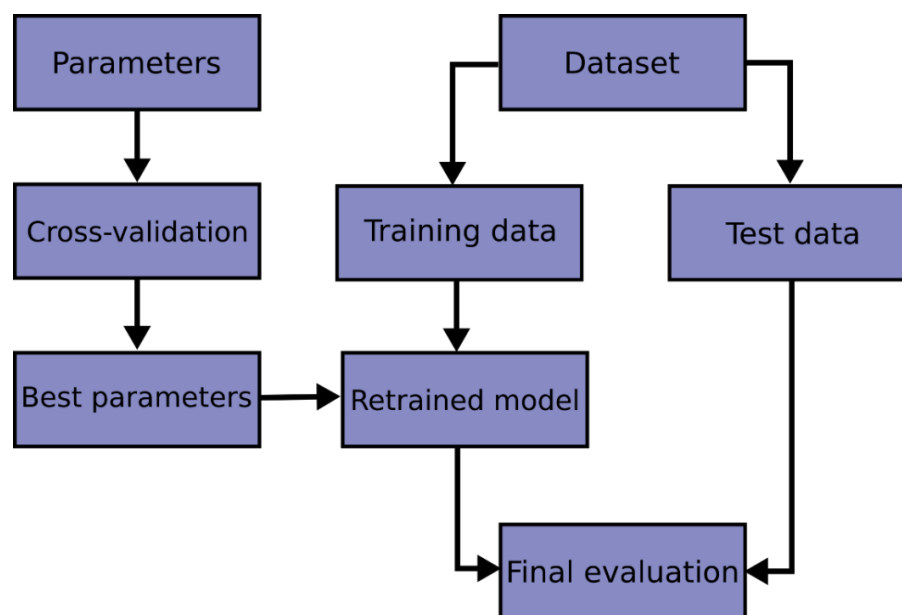


Figure 2. Flowchart indicating the actual processing steps followed in multivariate linear regression analysis.

2.5. Data Processing

To perform statistical data analyses and develop various graphical presentations, such as polar plots, time variation plots, and scatter plots, the statistical software R programming language [37] and its package Openair [38] were used.

3. Results

3.1. Overview of PM_{10} , $PM_{2.5}$, and BC Levels

The purpose of this section is to compare the PM_{10} , $PM_{2.5}$, and fine BC mass concentrations measured in Kenitra city to data obtained from the literature for different locations as given in Table S1. The table includes information on the types of sites, the research period, measuring techniques/methods, and reported concentration values. For our study period, the overall mean PM_{10} , $PM_{2.5}$, and BC mass concentrations were $50.1 \pm 17.7 \mu\text{g}/\text{m}^3$, $17.2 \pm 7.4 \mu\text{g}/\text{m}^3$, and $3.7 \pm 2.2 \mu\text{g}/\text{m}^3$, respectively. As to the PM_{10} mass concentrations, the annual mean was 4% higher than the limit of the Moroccan air quality standard values (decree n°2-09-286 setting standards for air quality and the modalities for air monitoring, 2009). The number of days exceeding the limit values of $50 \mu\text{g}/\text{m}^3$ was 33 days, accounting for 46% of the contribution to PM_{10} mean values. These days are often called PM_{10} pollution days [39]. Eighteen of these days were in summer, seven in autumn, five in winter, and three in spring, implying that the particulate matter pollution was higher in summer.

Regarding $PM_{2.5}$ mass, the annual mean of $17.2 \pm 7.4 \mu\text{g}/\text{m}^3$ exceeded the yearly World Health Organization (WHO) guidelines of $5 \mu\text{g}/\text{m}^3$ [4]. However, the daily $PM_{2.5}$ guidelines set by the WHO of $15 \mu\text{g}/\text{m}^3$ were exceeded in 30 out of the 70 measurement days. Five of them were in winter, three in autumn and spring, and none in summer, suggesting that the $PM_{2.5}$ levels were higher in winter. The observed PM_{10} and $PM_{2.5}$ values are considerably lower than those reported in a previous study by Tahri et al. [21], revealing that the area is less influenced by pollutant sources, particularly urban or industrial. They stated that the yearly average PM_{10} and $PM_{2.5}$ concentrations in Kenitra city from May 2007 to May 2008 were $161.1 \mu\text{g}/\text{m}^3$ and $50.7 \mu\text{g}/\text{m}^3$. In urban Meknes, Morocco, Ait Bouh et al. [40] found the annual average PM_{10} and $PM_{2.5}$ concentrations were 75.4 and $28.5 \mu\text{g}/\text{m}^3$, respectively. In contrast, Benchrif et al. [6] revealed that mean PM_{10} and $PM_{2.5}$ concentrations in urban/residential Tetouan, in northern Morocco in the Mediterranean

Basin, ranged between 25.6–31.1 and 13.7–18.6 $\mu\text{g}/\text{m}^3$ respectively, regarding the aerosol transport pathways.

In terms of BC, recorded mass concentrations are comparable to the range of values reported in earlier studies at urban locations in Tetouan, Morocco, ranging between 3.01 and 3.22 g/m^3 [6], at an urban background area in Krakow, Poland (3.5 $\mu\text{g}/\text{m}^3$) [22], and at an urban site in Barcelona, Spain (3.6 $\mu\text{g}/\text{m}^3$) [41]. However, the BC concentration values at our site are lower than the recorded values of 4.2 $\mu\text{g}/\text{m}^3$ in an urban area in Bern, Switzerland [42], 5.8 $\mu\text{g}/\text{m}^3$ at an urban site in Khulna, Bangladesh [43], and 6.5 $\mu\text{g}/\text{m}^3$ at an urban traffic site in Istanbul, Turkey [44].

3.2. Meteorological Conditions

The time series of the meteorological data derived from hourly measurements at Kenitra city in the July 2020–February 2021 period, obtained from NOAA Integrated Surface Database (ISD) meteorological observations, are shown in Figure S1. Table S2 provides a summary of descriptive statistics of 6 h meteorological parameters (T (temperature), P (pressure), RH (relative humidity), WS (wind speed), and Rainfall). The meteorological data shows that Kenitra is characterized by high temperature in summer (mid-August to September), with a daily mean ranging from 19.9–33.3 $^{\circ}\text{C}$, and the highest average of 23.5 $^{\circ}\text{C}$, followed by a warm autumn (mid-November to December) and a rather cold winter (January to mid-February) at 15.2 $^{\circ}\text{C}$ and 14.2 $^{\circ}\text{C}$, respectively, with an increase again in spring (April), reaching an average value of 16.76 $^{\circ}\text{C}$. The city is also known for high relative humidity (RH), generally higher than 70%. The highest RH values were recorded during winter (91.1% on average); the spring season showed a mean of 87.6%. Otherwise, Kenitra is usually windy, especially in summer, with wind speed averaging 3.4 m/s, against 2.8 m/s in both autumn and winter, and 2.6 m/s in spring. There was a predominance of south-westerly winds during the sampling period, with a frequency of more than 15%, while other wind directions, westerly and north-westerly in particular, were less pronounced (Figure 1). However, they remain dispersive wind regimes (>4 m/s), with a frequency greater than 10%. In short, the wind speed was higher in the summer and lower in the other seasons. From winter through summer and autumn, relative humidity dropped considerably. Seasonal variations showed that temperature values were comparatively higher in summer and lower in winter. The highest temperatures were experienced in August, while the highest rainfall levels were recorded in November and December.

3.3. PM Mass Characteristics

Figure 3 depicts the variation of PM_{10} and $\text{PM}_{2.5}$ mass concentrations over different seasons. According to a one-way ANOVA test using the collected data, PM_{10} and $\text{PM}_{2.5}$ showed statistically significant seasonal variations, and there was a difference between seasons (p -value > 0.01). Therefore, the daily PM_{10} and $\text{PM}_{2.5}$ concentrations varied depending on the season. The pattern of PM_{10} seasonal variation followed a similar trend to that of $\text{PM}_{2.5}$. The highest average PM_{10} concentration was mainly observed in the autumn (Table 1, Figure 3), ranging from 26.4 $\mu\text{g}/\text{m}^3$ to 95.4 $\mu\text{g}/\text{m}^3$ with an average of 61.4 ± 24.5 $\mu\text{g}/\text{m}^3$; this was followed by decreases in winter, reaching a minimum value of 16.22 $\mu\text{g}/\text{m}^3$, and an increase again in spring (21.4–88.0 $\mu\text{g}/\text{m}^3$), indicating an average of 44.1 ± 18.3 $\mu\text{g}/\text{m}^3$. Furthermore, higher values were also measured during summer, with an average of 54.6 ± 11.0 $\mu\text{g}/\text{m}^3$ and a range of 30.8–81.7 $\mu\text{g}/\text{m}^3$. In terms of $\text{PM}_{2.5}$, the highest values were observed in the autumn (21.18 ± 8.17 $\mu\text{g}/\text{m}^3$), followed by winter (17.09 ± 8.88 $\mu\text{g}/\text{m}^3$), spring (16.1 ± 9.2 $\mu\text{g}/\text{m}^3$), and summer (14.3 ± 3.3 $\mu\text{g}/\text{m}^3$). $\text{PM}_{2.5}$ concentrations ranged from 5.8 $\mu\text{g}/\text{m}^3$ in the spring to 37.2 $\mu\text{g}/\text{m}^3$ in the winter. The highest daily PM_{10} and $\text{PM}_{2.5}$ mass concentrations were reported in the autumn and winter, at 95.4 $\mu\text{g}/\text{m}^3$ and 37.2 $\mu\text{g}/\text{m}^3$, respectively.

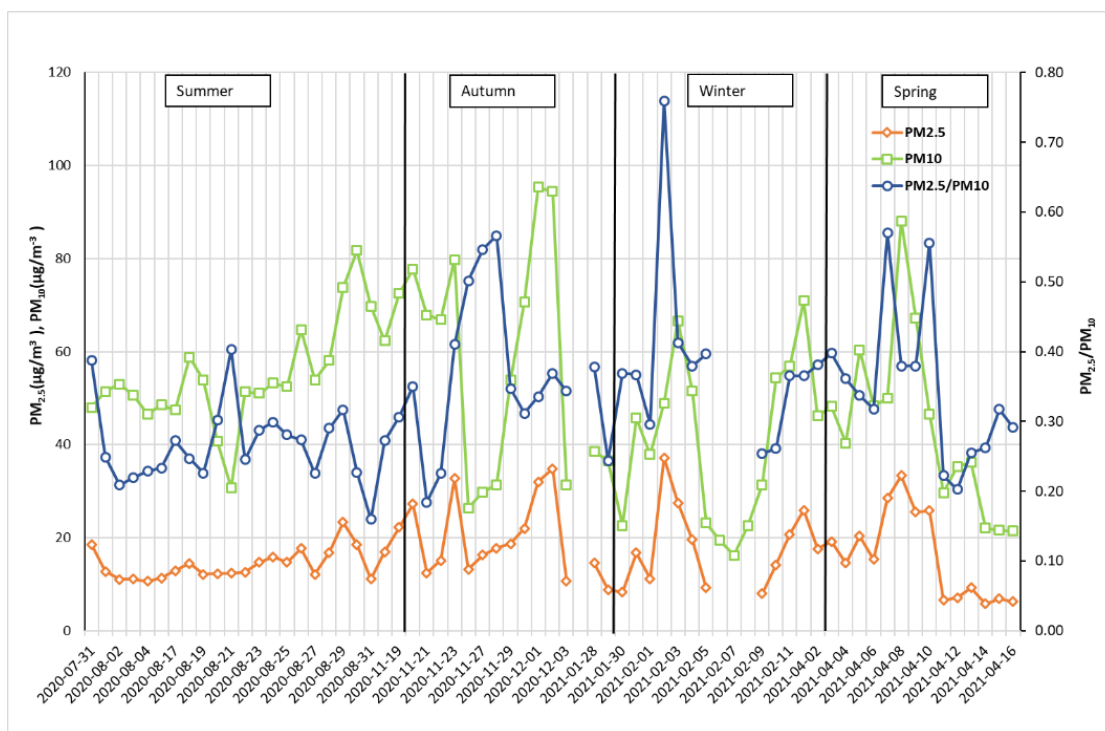


Figure 3. Temporal variations of ambient PM₁₀ and PM_{2.5} concentrations (μg/m³), and PM_{2.5}/PM₁₀ ratios, subdivided into seasons in Kenitra during the study period (2020–2021).

Table 1. Descriptive statistics of daily concentrations of PM₁₀, PM_{2.5}, and BC obtained between mid-July 2020 and mid-February 2021 (203 days). N stands for the number of total datasets used.

	Season	N	Mean	SD	Median	Min	Max
PM ₁₀ (μg/m ³)	Autumn	13	61.4	24.5	67.9	26.4	95.4
	Spring	15	44.1	18.3	46.2	21.4	88
	Summer	22	54.6	11	52.7	30.8	81.7
	Winter	16	40.2	17.1	38.3	16.2	71
	Annual	66	50.1	17.7	51.3	23.7	84
PM _{2.5} (μg/m ³)	Autumn	13	21.2	8.2	18.7	10.8	34.8
	Spring	15	16.1	9.2	15.4	5.8	33.4
	Summer	22	14.3	3.3	12.9	10.6	23.4
	Winter	13	17.1	8.9	14.6	8	37.2
	Annual	63	17.2	7.4	15.4	8.8	32.2
PM _{2.5} /PM ₁₀	Autumn	13	0.37	0.11	0.35	0.18	0.57
	Spring	15	0.35	0.11	0.34	0.20	0.57
	Summer	22	0.27	0.06	0.26	0.16	0.40
	Winter	13	0.37	0.13	0.37	0.24	0.76
	Annual	63	0.34	0.10	0.33	0.20	0.57
BC (μg/m ³)	Autumn	14	3.3	2.8	2.7	1.1	11.9
	Spring	15	2.9	0.9	2.9	1.5	4.7
	Summer	22	6.3	4.2	5.3	2	19.5
	Winter	16	2.5	0.7	2.5	1.2	3.7
	Annual	67	3.7	2.1	3.3	1.4	10
BC/PM _{2.5}	Autumn	14	0.18	0.14	0.13	0.03	0.53
	Spring	15	0.25	0.15	0.20	0.10	0.55
	Summer	22	0.43	0.21	0.44	0.15	0.84
	Winter	16	0.18	0.10	0.17	0.05	0.36
	Annual	67	0.26	0.15	0.23	0.08	0.57

Table 1 and Figure 3 demonstrate clearly that peak PM_{10} and $PM_{2.5}$ levels occurred in the autumn and spring; however, elevated $PM_{2.5}$ mean values were also reported in the winter. There are three primary reasons for this enhancement. One factor is the relatively decreased precipitation in winter (6.3% of days with rainfall) compared to autumn (35.7%) and spring (13.3%), indicating that the wet-scavenging effect of the rain was smaller in winter. The other is attributed to more stable atmospheric conditions due to lower wind speed in winter (2.9 m/s) compared to summer (3.4 m/s). The third reason is connected to the air masses arriving at the sampling site, implying that regional and long-range emission sources likely contribute to the observed seasonal variations. These were further supported by CWT analyses (Figure 4), which also showed the influence of local and regional activities during the autumn and spring period. CWT analysis showed a clear seasonal change in the mean air mass pathways. For instance, during the winter season, the highest WCWT (weighted concentration-weight trajectory) values were distributed in western Morocco and the Atlantic Ocean, and large areas were the main contribution sources associated with PM_{10} concentrations less than $15 \mu\text{g}/\text{m}^3$. In this season, the major fraction of air mass arriving at our site originated over the Atlantic Ocean region, during which the seasonal mean PM_{10} concentration was also the lowest ($<40 \mu\text{g}/\text{m}^3$). Figure S2 depicts the percentage of back-trajectory clusters of incoming air masses at Kenitra throughout various seasons of the sampling period. During the autumn season, the maximum WCWT PM_{10} was higher than in winter. The CWT model identified that the strong contributions were from local sources in addition to the east and central region of Morocco. In autumn, where PM_{10} was quite significant ($61 \mu\text{g}/\text{m}^3$, on average), the major air mass pathways ($\sim 37\%$) moved slowly over the local area, while a small fraction ($\sim 12\%$) indicated possible long-transported aerosols from the eastern part of Morocco. In summer and spring, the air quality in Kenitra is affected by pollutants emitted from the Iberian coast and northern Morocco, with high WCWT values of about 25–35 and 20–30 $\mu\text{g}/\text{m}^3$, respectively. In Figure 4, we found that the CWT maps of $PM_{2.5}$ were very similar to the PM_{10} CWT maps. In addition, the east and north of Morocco and local sources showed high WCWT $PM_{2.5}$ values of about 8–14 $\mu\text{g}/\text{m}^3$. The potential source areas associated with the high WCWT values for $PM_{2.5}$ were approximately 6–8, 8–12, and 10–14 $\mu\text{g}/\text{m}^3$ in summer, spring and autumn, and winter, respectively. CWT maps of $PM_{2.5}$ across four seasons in Kenitra are illustrated in Figure S3.

Annual $PM_{2.5}$ to PM_{10} mass ratios were approximately 0.34, with seasonally averaged ratios ranging from 0.27 in summer to 0.37 in autumn and winter. The ratio has a mean value of 0.35 in spring. As shown in Figure 3, this seasonal trend in PM ratio results from the seasonal variations in PM levels and emissions across all seasons. The low summer $PM_{2.5}/PM_{10}$ ratios (0.27) could be linked to the predominance of coarse particles, which could have come from local pollution sources in the city studied. Abuelgasim and Farahat [45] stated that the difference in PM ratio magnitude depends on the season. In Kenitra, the PM ratio peak is usually reached in the autumn and winter months, while in the Emirate of Abu Dhabi it is usually reached in summer [45], and in urban Chinese cities in winter [11]. The magnitude of the obtained $PM_{2.5}/PM_{10}$ mass ratios is quite similar to 0.36 compared to earlier studies in Kenitra (2007–2008) reported by Zghaid et al. [46], but somewhat lower than that of 0.39 reported by Ait Bouh et al. [40] in Meknes, northern Morocco, in the Middle Atlas (2007–2008). It is significantly low compared to similar ratio values reported in other locations, such as the value of 0.58 for Khulna, Bangladesh [43], and 0.61 for Bern, Switzerland [42].

3.4. BC Mass Characteristics

Daily mean BC concentrations ranged from $1.05 \mu\text{g}/\text{m}^3$ to $19.5 \mu\text{g}/\text{m}^3$ (Table 1), with significant seasonal variation (Figure 5). Average summer BC concentrations ($6.3 \mu\text{g}/\text{m}^3$) were twice as high as autumn ($3.3 \mu\text{g}/\text{m}^3$). Summer BC concentrations averaged 62% higher than the one-year mean of $3.9 \mu\text{g}/\text{m}^3$, while autumn, winter, and spring averages were 16%, 24%, and 35% lower, respectively, than the one-year average. Table 1 shows

that overall BC concentrations were higher in August and November, while they were lower during other months over the year, with different magnitudes. Monthly averaged BC mass concentration varies, with the maximum in August ($6.2 \mu\text{g}/\text{m}^3$) and minimum in December ($1.2 \mu\text{g}/\text{m}^3$). The highest peaks of BC of $19.5 \mu\text{g}/\text{m}^3$ and $11.9 \mu\text{g}/\text{m}^3$ were observed on 29 August and 19 November 2020, respectively. The higher concentration of BC in August and the lower in December is mainly due to meteorological impacts such as relative humidity, temperature, wind direction, and removal by rainfall [47].

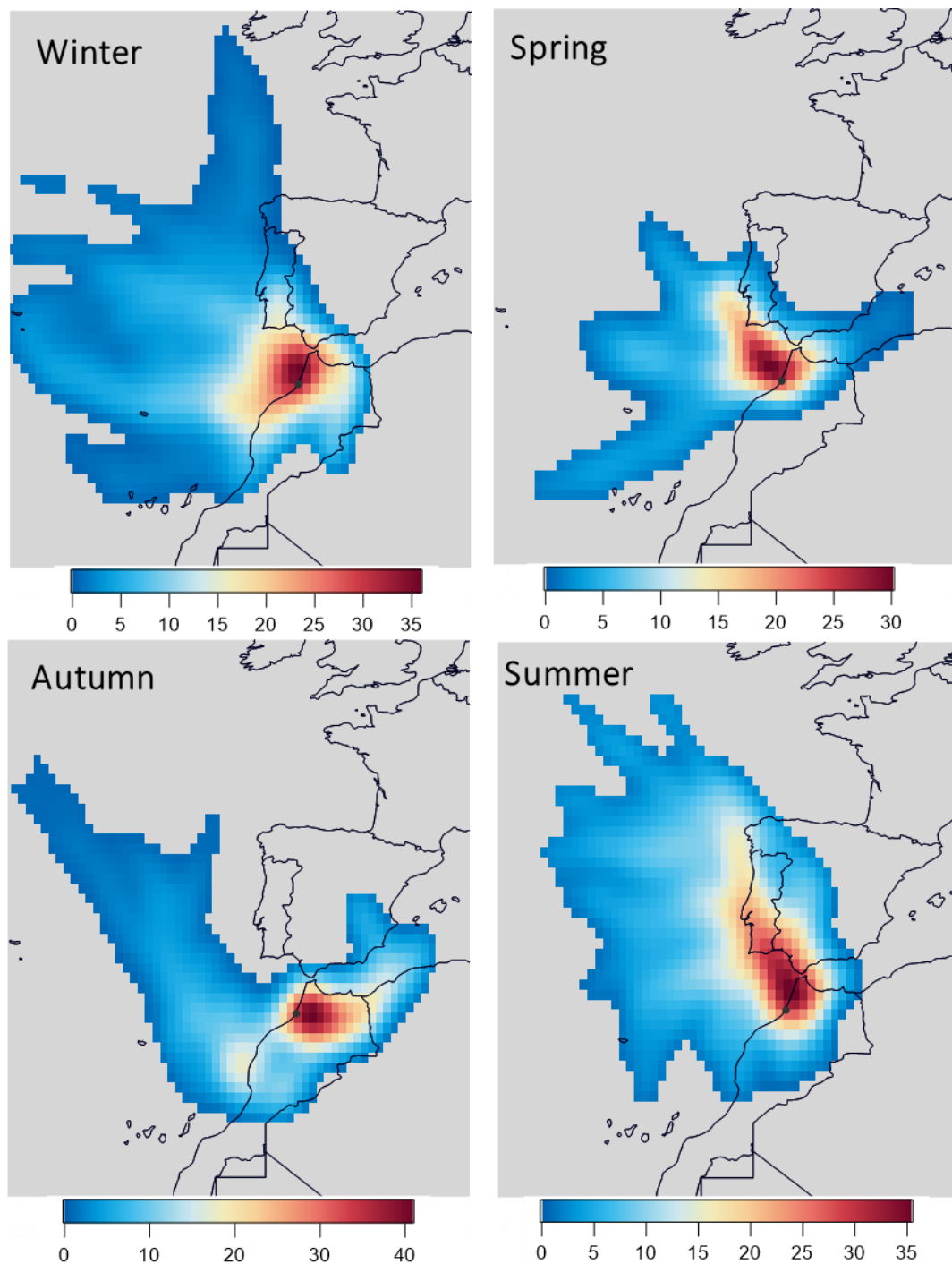


Figure 4. CWT maps for spring, summer, autumn, and winter in Kenitra. The red areas represent the main potential source-areas affecting PM_{10} concentrations. Scales are in $\mu\text{g}/\text{m}^3$.

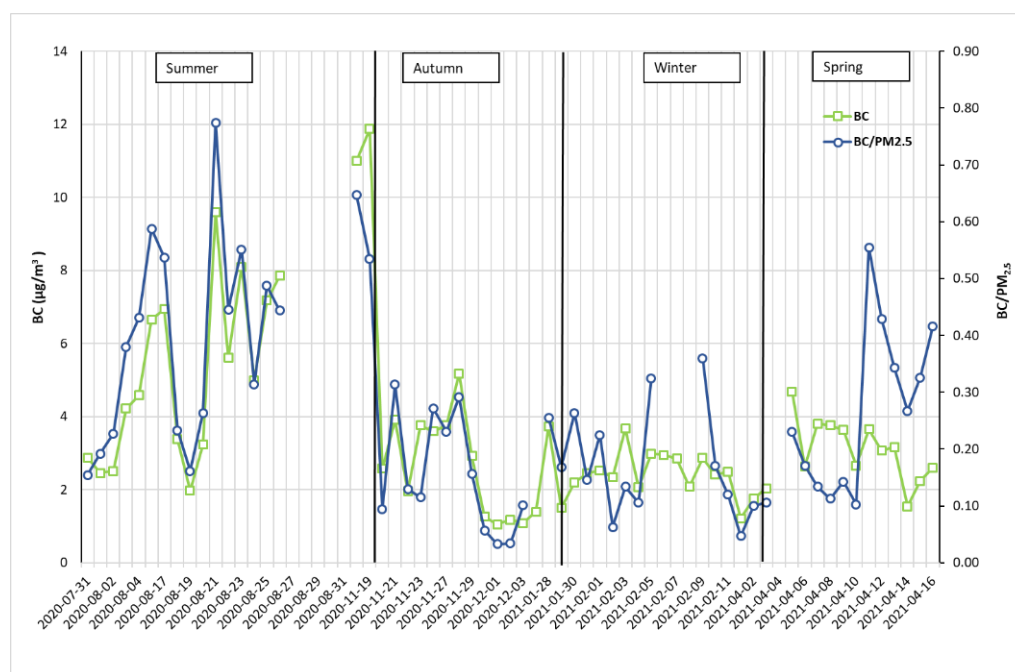


Figure 5. Temporal variations of ambient BC concentrations ($\mu\text{g}/\text{m}^3$) and BC/PM_{2.5} ratios subdivided into seasons in Kenitra during the study period (2020–2021).

The one-way ANOVA test results revealed that the difference in BC values between days was not statistically significant, while the difference in BC concentrations between seasons was statistically significant at a p -value < 0.001 . The daily characteristics of BC indicated that the main source of BC had less diurnal variation, i.e., road traffic, whereas the seasonal characteristics show that the BC-contributing sources had more seasonal fluctuations, e.g., biomass burning and emissions from long-range transport [48]. As previously mentioned, BC is a by-product of incomplete combustion that is emitted in large quantities from diesel-powered engines. Heavy-duty diesel-powered trucks traveling along the national road and the highway that passed near the sampling site may contribute more to the BC values. Furthermore, the impact of meteorological conditions on the seasonal variation of BC is also distinguishable. High BC concentrations in summer could be attributed to meteorological conditions, such as relative dryness (low humidity) and less rainfall. Compared to the summer, the BC concentration was lower in autumn, possibly due to the frequent rainfall events in this season, accounting for 35.7%, and of the entire sampling period. Rain has a wet removal effect on BC and greatly reduces BC concentration. The analysis of the back-trajectory patterns (Figure S2) showed a high potential contribution of the long-range transport aerosols in combination with primary emissions of carbonaceous components released by the maritime activity in the Atlantic region before reaching the study area.

Figure 5 depicts the variation in BC/PM_{2.5} mass ratios. The average BC/PM_{2.5} ratio was 27% and ranged between 3% and 84%. Summer had the largest average ratio of 43%, with the lowest PM_{2.5} mass ($14.3 \mu\text{g}/\text{m}^3$), but winter and autumn had the lowest BC/PM_{2.5} ratios (18%). It is known from prior studies that the BC abundance in PM_{2.5} is influenced by many factors, including the sequence of pollution events, the mixing of pollution sources, and meteorological conditions [17,49]. The average ranges of BC/PM_{2.5} obtained at our monitoring sites were comparable to those previously reported for Los Angeles, California, i.e., BC accounts for 21% of PM_{2.5} [50]. The values recorded were higher than the values reported for urban Helsinki, Finland, where Viidanoja et al. [51] found BC as 14% of PM_{2.5}. Yu et al. [17] found BC to PM_{2.5} ratios ranging from 5.1% to 5.6%, depending on the season in urban Beijing, China. Zhang et al. [49] found an average BC/PM_{2.5} value of 3.04% in Lanzhou in China, with a value of 4.04% in winter and 2.06% in summer.

3.5. Relationship between PM₁₀, PM_{2.5}, BC, and Meteorological Factors

3.5.1. Univariate Correlation Analyses

The relationship between PM and meteorological variables can sometimes be complex and not linear [52]. Many studies have argued that PM and BC seasonal variation has a substantial association with meteorological factors. Kliengchuay et al. [53] (in Lamphun, Thailand) and Krampah et al. [54] (in Tarkwa, Ghana) found that PM₁₀ was negatively correlated to relative humidity, temperature, and wind speed. Chen et al. [55] found in urban Nanjing (China) a negative correlation between PM_{2.5} concentration and wind speed, temperature, relative humidity, and precipitation. Other studies [55,56] demonstrated that the correlations between particulate matter concentration and meteorological factors might be varied with the seasons. Zhang et al. [49] (in Lanzhou, China) noticed that BC concentrations in PM₁, PM_{2.5}, and PM₁₀ were higher in winter due to favorable meteorology for accumulating pollutants, whereas precipitation had an important role in scavenging pollutants, resulting in reduced BC concentrations in summer. In this study, the correlation matrix between BC, PM_{2.5}, PM₁₀, and meteorological factors, namely wind speed (WS), temperature (T), rainfall, relative humidity (RH), and pressure (P), was investigated. Various studies have examined the impact of meteorology on PM, taking into account the lag effects of meteorological factors using a non-linear model [57,58]. In our case, using a simple analysis method, it was found that the 1–3 lag day scenario was the most suitable. In fact, the highest meteorological effects typically occurred on day one (lag day 0) and then rapidly decreased throughout the lag period. However, we have found that the lag effect of meteorology on PM pollution varies depending on the meteorological variable. Indeed, the lag effects (1–3 days earlier) of meteorological variables were taken into account, because preceding weather conditions may influence later air pollutant concentrations [59,60]. The meteorological factors that had the strongest association with BC, PM_{2.5}, and PM₁₀ from lag0 (current value) to lag3 (value 3 days previously) were discussed. Only Spearman correlation coefficients with significant statistics at the 0.01 and 0.05 levels were considered. Table 2 displayed the spearman correlation coefficient for meteorological and air pollution variables that were delayed by 0–3 days.

Table 2. Spearman correlation coefficient between meteorological and air pollution variables for Kenitra delayed by 0–3 days. Correlation with a significant statistic at a 99% confidence level is denoted by * and significant at 95% by **. The numbers in parentheses highlight the lag days with the strongest correlation.

	Seasons	T (°C)	WS (m/s)	RH (%)	Rainfall (mm)	P (hPa)
BC (µg/m ³)	Spring	−0.12 (2)	0.39 (3)	0.42 (0)	−0.42 (0)	−0.38 (3)
	Summer	−0.61 * (0)	−0.08 (3)	−0.70 * (2)		−0.24 (2)
	Autumn	−0.28 (2)	0.44 (1)	0.16 (2)	−0.45 (3)	0.77 * (3)
	Winter	−0.24 (0)	−0.46 (2)	−0.30 (3)	−0.31 (2)	−0.38 (1)
	Whole	0.56 * (3)	0.39 * (1)	−0.40 * (2)	0.33 ** (3)	−0.33 * (1)
PM _{2.5} (µg/m ³)	Spring	0.19 (2)	0.54 ** (1)	−0.24 (0)	−0.49 ** (0)	−0.29 (3)
	Summer	−0.59 * (3)	−0.48 ** (2)	−0.66 * (3)		−0.16 (2)
	Autumn	0.39 (0)	−0.23 (0)	0.47 (2)	0.55 (3)	−0.37 (2)
	Winter	−0.54 ** (1)	−0.38 (1)	−0.45 (3)	−0.52 (3)	0.59 ** (3)
	Whole	−0.20 (1)	−0.19 (0)	−0.12 (1)	−0.10 (0)	0.11 (0)
PM ₁₀ (µg/m ³)	Spring	−0.13 (0)	0.36 (3)	−0.25 (3)	−0.61 ** (1)	−0.31 (3)
	Summer	−0.23 (3)	−0.59 * (3)	−0.32 (1)		−0.27 (0)
	Autumn	0.60 ** (1)	−0.49 (0)	−0.63 ** (1)	−0.74 * (0)	0.69 * (0)
	Winter	0.26 (0)	−0.59 * (0)	0.51 ** (1)	−0.43 (1)	0.50 ** (2)
	Whole	0.33 * (3)	0.30 ** (3)	−0.49 * (3)	−0.38 * (0)	−0.20 (3)

Correlation analysis during the whole period indicated that BC concentrations were significantly correlated with prior day wind speed ($r = 0.39$, p -value < 0.01 , lag1), prior day air pressure ($r = -0.33$, p -value < 0.01 , lag1), temperature 3 days prior ($r = 0.56$, p -value < 0.01 , lag3), relative humidity 3 days earlier ($r = -0.40$, p -value < 0.01 , lag3) and rainfall 3 days earlier ($r = 0.33$, p -value < 0.05 , lag3). While an insignificant association is observed between PM_{10} and air pressure, the strongest correlations were exhibited with relative humidity 3 days earlier ($r = -0.49$, p -value < 0.01 , lag3), rainfall on the day of measurement ($r = -0.38$, p -value < 0.01 , lag0), wind speed 3 days prior ($r = 0.30$, p -value < 0.05 , lag3), and temperature 3 days earlier ($r = 0.33$, p -value < 0.01 , lag3). Individual correlations between $PM_{2.5}$ and all meteorological variables, on the other hand, were completely missing.

All over the seasons under study, PM_{10} concentrations were significantly correlated with relative humidity, which was negatively associated in autumn ($r = -0.63$, p -value < 0.05 , lag1) and turned to positive in winter ($r = 0.51$, p -value < 0.05 , lag1), implying that winter humidity had a prominent influence on PM_{10} concentrations. Thus, the greater the winter humidity, the easier it is to induce serious pollution [31]. However, relative humidity was shown to be negatively correlated with $PM_{2.5}$ only in summer ($r = -0.66$, p -value < 0.01 , lag3). These correlation coefficients indicated that there was an increase in the humidity effect with the number of lag days, and the relative humidity 3 days earlier was substantially associated with PM_{10} and $PM_{2.5}$ concentrations. The correlation with the relative humidity 1–3 days earlier was the strongest (Table 2), and the correlations in summer were stronger than those in autumn and winter, which was likely due to the varied effects of humidity on the concentrations of fine and coarse particles. Munir et al. [61] and Barmpadimos et al. [62] reported that PM concentrations increase with low humidity. However, after humidity reached a sufficient level, the PM concentrations decreased, which is ascribed to the fact that particles accumulate and then eventually lead to a dry deposition on the ground. For instance, previous studies [63] found that ultrafine particle concentrations were higher during rainy seasons.

The correlation analysis also reveals the association of PM_{10} and $PM_{2.5}$ with wind speed, rainfall, pressure, and temperature. The temperature 1 day earlier correlated positively with PM_{10} in autumn ($r = 0.60$, p -value < 0.05 , lag1) and negatively with $PM_{2.5}$ in winter ($r = -0.54$, p -value < 0.05 , lag1) and summer ($r = -0.59$, p -value < 0.01 , lag3). Temperature is one of the dominant factors governing the diffusion ability of the atmosphere, since it may alter the vertical transport and diffusion capabilities of the atmosphere [64]. As the temperature increases, vertical convection becomes stronger, and the vertical transport capacity of the atmosphere increases. This phenomenon speeds up the exchange of atmospheric particles between the ground and higher altitudes. Luo et al. [31] found in Haerwusu Open-pit Coal Mine, China, that the influence of temperature on PM concentration changes by the month. The inverse relationship with temperature in winter can lead to high $PM_{2.5}$ concentrations through condensation of volatile compounds [62], while the positive effect in autumn can affect particle formation. Additionally, the high temperature might promote photochemical reaction between precursors [65]. In Kenitra, Tahri et al. [21] demonstrated a strong positive effect of temperature on the concentration of coarse particles.

Rainfall was significantly negatively correlated with PM_{10} in spring ($r = -0.61$, p -value < 0.05 , lag1) and autumn ($r = -0.74$, p -value < 0.01 , lag0), and with $PM_{2.5}$ in spring ($r = -0.49$, p -value < 0.05 , lag0). $PM_{2.5}$ concentration drop with increasing rainfall is likely due to the washout effect and wet deposition by rainfall (Figures 3 and S1). Rainfall, according to Wang and Ogawa [65], can effectively reduce PM mass concentrations through wet deposition and can remove particles, especially small-sized ones.

Similarly, wind speed correlates with PM_{10} in winter ($r = -0.59$, p -value < 0.01 , lag0) and summer ($r = -0.59$, p -value < 0.01 , lag3), and with $PM_{2.5}$ in summer ($r = -0.60$, p -value < 0.01 , lag2) and in spring ($r = 0.54$, p -value < 0.05 , lag1). These distinct effects of wind speed on $PM_{2.5}$ concentration suggest that when wind speed is low (average

2.7 m/s in spring), pollutants can be blown away in a given geographic area, preventing PM dispersion and thus intensifying its deposition and accumulation. Nevertheless, with sufficiently high wind speed (3.4 m/s in summer, on average), large amounts of pollutants can be transported from afar [66]. Dung et al. [67] stated that low wind speeds and different directions caused PM₁₀ to spread slowly and then increased its concentrations. Zhang et al. [68] showed that under conditions of low wind speed and a highly stable atmosphere, horizontal diffusion and vertical disturbance are less pronounced, although air pollutant concentrations increase significantly.

In terms of atmospheric pressure, the correlation coefficient increased in winter with the number of lag days, but the opposite occurred in autumn. Atmospheric pressure 2–3 days earlier was strongly correlated with current PM₁₀ and PM_{2.5} concentrations. The unstable atmospheric environment in winter likely accelerated the change in particulate matter concentration [39].

BC concentration, temperature, and relative humidity showed a significant correlation only in summer (correlation in other seasons was insignificant), and air pressure did in autumn. Correlation coefficients were with air temperature ($r = -0.61$, p -value < 0.01 , lag0), relative humidity 2 days earlier ($r = -0.70$, p -value < 0.01 , lag2), and pressure 3 days earlier ($r = 0.77$, p -value < 0.01 , lag3). In contrast to numerous studies confirming the negative correlation between BC concentrations and wind speed in some urban areas [69–72], no significant association was found in our work. This is consistent with findings reported by Wang et al. [73] at a rural site near Beijing, suggesting that emissions from local sources were very limited at their site. As shown in Figure S4, the autumn high WCWT BC concentrations were clearly distributed in the eastern areas of Morocco. These high potential areas could be caused by polluted aerosols traveling into Kenitra from other cities, as well as local activities such as industry and road traffic. Interestingly, high summer WCWT BC concentrations from the Iberian region and the Strait of Gibraltar in summer, winter and spring seasons could be partially explained by a significant contribution from the ship emissions sector [5,74]. An inverse relationship between temperature and BC could be due to favorable conditions for condensation of fresh traffic exhaust emissions, semi-volatile species during winter, and secondary organic compounds produced by photochemistry reactions in summer [75]. Furthermore, higher temperature increases the buoyancy of air parcels and stretches the atmospheric boundary layer, which contributes to the dilution of pollutants [76]. What is striking about this correlation investigation is that high BC concentrations ($6.3 \mu\text{g}/\text{m}^3$, on average) were found in summer. This period is associated with high wind speeds (3.4 m/s) compared to winter (2.9 m/s), moderate relative humidity (average 76%, with a range of 49% to 84%), and no episodes of rainfall. Rajeevan et al. [47] argued that high humidity could cause the coagulation of particles to become heavier, inferring rapid deposition; then, concentrations decrease, while the lower summer relative humidity may contribute to an increase in BC concentrations. According to Wang et al. [77], carbonaceous aerosols tend to agglomerate in the 45–60% relative humidity range and from $-5 \text{ }^\circ\text{C}$ to $0 \text{ }^\circ\text{C}$, having higher concentrations than other temperatures and humidity ranges. On the other hand, the BC concentrations did not show a significant relationship with rainfall. Rainy days accounted for about 12% of the total sampling, suggesting that rainfall had relatively insignificant effects on BC concentrations.

In brief, until this stage, our results were consistent with previous studies, mentioned above, showing that correlations between aerosol concentrations (PM₁₀, PM_{2.5}, and BC) and meteorological factors are significant and may vary by season. In addition, the lagging effect of meteorology on PM and BC pollution varies depending on the meteorological variable. For example, RH was negatively associated with PM₁₀ in autumn and became positive in winter, while it was negatively correlated with PM_{2.5} only in summer. Then, the RH effect increases with the number of lag days, i.e., the correlation of RH 3 days earlier (lag3) was substantially associated with PM₁₀ and PM_{2.5} concentrations. Concerning BC concentrations, a negative correlation was found with temperature (lag0) and relative humidity (lag2), while air pressure (lag3) showed a positive correlation.

3.5.2. Multivariate Linear Regression Analyses

As discussed previously, the univariate correlation analysis showed that not all considered meteorological variables are highly correlated with PM₁₀, PM_{2.5}, and BC and influence their changes. Thus, we conducted a multivariate regression analysis (MLR) to quantify whether the impact of metrology would change in a multivariate analysis. Numerous studies have used multiple linear regression analysis in the field of air pollution and concluded that MLR provides information on the impact of multiple meteorological variables on PM₁₀, PM_{2.5}, and BC levels [30,31,56,78,79]. In our work, the MLR method was applied only at the annual scale, since the significant correlation between meteorological variables (temperature, wind speed, relative humidity, pressure, and rainfall), and PM₁₀, PM_{2.5}, and BC, when the lag effects were not considered, was observed throughout the whole sampling period. According to the first and second steps introduced in Section 2.3, highlighting the most strongly correlated variables, a shortlist of meteorological parameters was selected for the following regression analysis. Table 3 shows the obtained test, training, and cross-validation (CV) root mean square error (RMSE) and correlation coefficient (r²) values.

Table 3. Statistical characteristics of the best model prediction for PM₁₀, PM_{2.5}, and BC.

	Best-Fitting Model	RMSE Training	RMSE Test	RMSE CV	R ² Training	R ² Test	R ² CV
BC	Logarithmic	3.03	1.47	0.52	18.56%	46.65%	33.46%
PM ₁₀	Logarithmic	16.77	11.72	0.34	18.29%	33.67%	42.33%
PM _{2.5}	Logarithmic	7.93	5.79	0.45	10.13%	4.13%	37.90%

To establish the best-fitting model, several multiple regression models were examined. It was found that fitting the non-linear model to the meteorological variables produced the best results. The suggested regression equation between PM₁₀, PM_{2.5}, BC, and meteorological variables can be written as shown in Equations (2)–(4), respectively. It can be noted that two meteorological parameters have a significant impact on the PM₁₀ and BC concentrations. These later were both negatively affected by relative humidity, while wind speed was positively correlated with BC and negatively with PM₁₀. However, PM_{2.5} concentrations were positively proportional to the temperature degrees.

$$\log PM_{10} = -6.899 \log WS - 1.152 \log RH + 165.367 \tag{2}$$

$$\log PM_{2.5} = 0.55 \log T + 26.90 \tag{3}$$

$$\log BC = 0.60 \log WS - 0.17 \log RH + 16.86 \tag{4}$$

3.5.3. Relationship between PM₁₀, PM_{2.5} and BC Levels and Wind Direction

To identify and determine the origins of PM₁₀, PM_{2.5}, and BC reaching the sampling site from different directions, bivariate polar plots were used by computing the mean concentration for wind speed and direction bins [80]. Figures 6 and 7 present polar plots of PM₁₀, PM_{2.5}, and BC concentration for the four seasons (spring, winter, summer, and autumn) at Kenitra city.

In autumn, easterly winds caused the highest average PM₁₀ concentrations, followed by south-westerly winds. Southwest winds with a faster speed (>4 m/s) in winter produced the lowest average PM₁₀ concentrations. In summer and spring, northwest winds were more frequent but slower (average > 2.5 m/s). In general, easterly winds carry PM₁₀ from road traffic processes and highways, while north-westerly winds carry pollutants from industrial processes near the sampling site. The southwest winds have a higher speed and bring local fine dust with them from the residential neighbors. In addition, polar plots showed that a major source of PM₁₀ is located near the monitoring site, which coincides with road traffic and is highly dependent on dust-raising processes on the road surface. In summary, seasonal fluctuations in PM₁₀ are closely linked to meteorological parameters

such as wind direction and wind speed, which favorably or negatively influence particulate matter pollution.

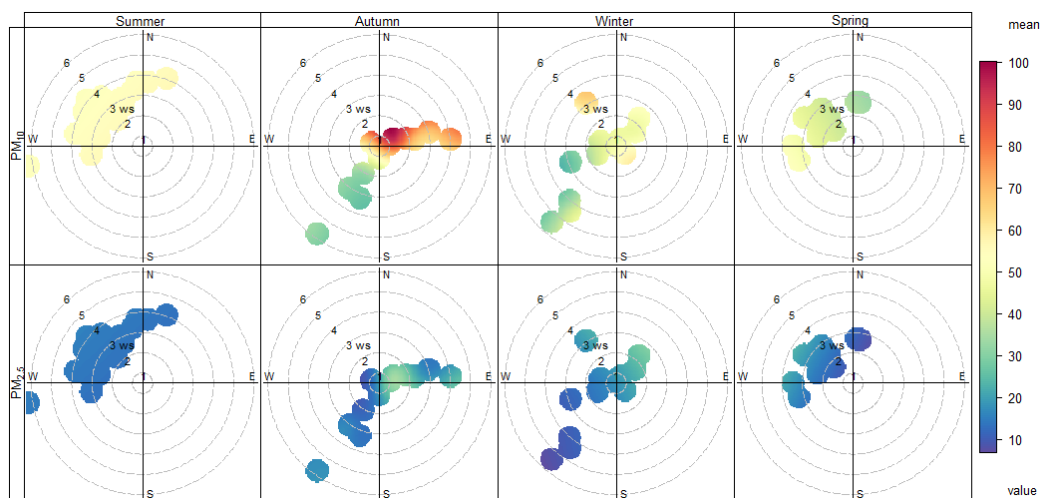


Figure 6. Polar plots of PM_{10} and $PM_{2.5}$ concentrations for four seasons (spring, winter, summer, and autumn) in the city of Kenitra. The average PM concentration ($\mu\text{g}/\text{m}^3$) is coded according to the color scale shown on the right. The dashed circular grey lines show the wind speed scale.

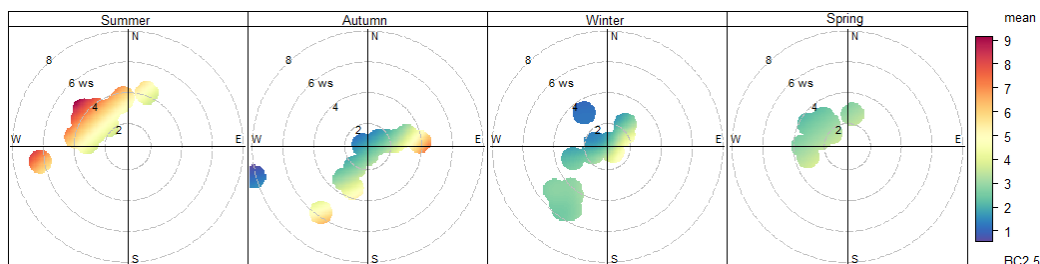


Figure 7. Polar plots of BC concentrations for four seasons (spring, winter, summer, and autumn) in the city of Kenitra. The average BC concentration ($\mu\text{g}/\text{m}^3$) is coded according to the color scale shown on the right. The dashed circular grey lines show the wind speed scale.

As shown in Figure 7, the high summer BC concentrations were mainly caused by the northwest winds, followed by southwest and north-easterly winds, noting that high BC concentration was associated with high wind speeds (>4 m/s). Meanwhile, the main sources of BC mass concentration in autumn were the southwest and east winds, generating a high average BC from high wind speeds. In winter, southwest winds were considered the main source of BC, with different wind speed scales from 0 to 6 m/s, followed by northeast and northwest winds. However, high BC values in winter were associated with low wind speeds (<2 m/s), indicating a strong contribution from local sources. BC in spring is almost the same as in summer but at lower levels. It could be noted that low wind speed (<2 m/s) is associated with higher BC concentration. Overall, the major BC sources were located near the sampling site with wind speeds of less than 2 m/s, indicating that the main production of BC was from a local source under relatively stable atmospheric conditions.

4. Conclusions

This paper shows the principal features of the seasonal variation of aerosol concentrations (PM_{10} , $PM_{2.5}$, and BC) in Kenitra, Morocco, from July 2020 to April 2021 and their relationship with meteorological factors using univariate and multivariate linear regression analyses. The annual concentrations of PM_{10} and $PM_{2.5}$ show clear seasonality, with the maximum in the autumn, while the minimum was observed in the winter for PM_{10} and

in the summer for $PM_{2.5}$. The highest level was likely due to stable atmospheric conditions (low wind speed) and the contribution of source emissions throughout air masses arriving at the sampling site. The average $PM_{2.5}/PM_{10}$ ratio of 0.34 could be related to the predominance of coarse particles, which could originate from local pollution sources at the studied location. Correlation analyses revealed that aerosol (PM_{10} , $PM_{2.5}$, and BC) seasonal variation and meteorological variables are strongly coupled. PM_{10} was negatively associated with relative humidity in autumn, and it turned positive in winter, while $PM_{2.5}$ was shown to be negatively correlated only in summer. The $PM_{2.5}$ concentrations under the dominance of a westerly wind in summer (of approximately 3.4 m/s) were approximately 1.1–1.5 times lower than under other wind directions. Rainfall, on the current day and the next day, was negatively correlated with PM_{10} in spring and autumn, and with $PM_{2.5}$ in spring. In terms of BC concentration, the temperature on the day of measurement and relative humidity 2 days earlier showed a negative correlation only in summer, although air pressure 3 days earlier had a positive correlation in autumn. The most striking feature of this figure is that higher BC concentrations are observed during the summer season, associated with high temperature, high wind speed, moderate relative humidity, and no episodes of rainfall. This may be attributable to the high local and long-range transported aerosol source contribution and the low summer relative humidity. The multivariate correlation analyses revealed that the relationship between particulate matter (PM_{10} , $PM_{2.5}$, and BC) and meteorological variables is not linear. Relative humidity had a negative impact on both PM_{10} and BC concentrations, while wind speed had a positive impact on BC but a negative impact on PM_{10} . However, $PM_{2.5}$ concentrations are inversely related to temperature. Furthermore, the CWT model shows obvious spatial distributional features and seasonal differences in potential source areas affecting $PM_{2.5}$, PM_{10} and BC levels in Kenitra.

This study provides detailed insight into how meteorological variables can be used to understand the features of particulate (PM_{10} and $PM_{2.5}$) and carbonaceous (BC) aerosols and their seasonal differences in the urban area of Kenitra. The current study, despite showing a strong correlation between meteorological and air pollution variables in Kenitra, has the following limitations. First, the measurement campaign was limited in time (15 days/season) and space (1 fixed station). Secondly, the inclusion of datasets about emissions from some local sources of potential importance (e.g., traditional public bathhouses, wood combustion, and mobile sources circulating inside the city) would be an interesting research contribution. Future attempts should consider more observation locations and longer period data to compare the relationship between aerosol levels and meteorological variables, including some other meteorological factors.

Supplementary Materials: The following supporting information can be downloaded at: <https://www.mdpi.com/article/10.3390/atmos14010162/s1>, Figure S1. Hourly temperature ($^{\circ}C$), rainfall (mm), wind speed (m/s), air pressure (hPa), and relative humidity (percent) time series for Kenitra city from mid-July 2020 to mid-February 2021, retrieved from NOAA Integrated Surface Database (ISD) meteorological data; Figure S2. Typical back-trajectories arriving at Kenitra from mid-August 2020 to mid-February 2021 are characterized into six backward trajectory clusters and categorized by season: (a) winter (January–mid-February), (b) spring (April), (c) summer (mid-August–September), and (d) autumn (mid-November–December); Figure S3: CWT maps for spring, summer, autumn, and winter at Kenitra. The red areas represent the main potential source-areas affecting $PM_{2.5}$ concentrations. Scales are in $\mu g/m^3$; Figure S4: CWT maps for spring, summer, autumn, and winter at Kenitra. The red areas represent the main potential source-areas affecting BC concentrations. Scales are in $\mu g/m^3$; Table S1. PM_{10} , $PM_{2.5}$, and BC values recorded in Kenitra compared to those reported in other locations, with an emphasis on urban-impacted areas. The table is ordered according to PM_{10} mass concentration. * Calculated from reported $PM_{2.5}$ and PM_{10} values; - data unavailable; Table S2. Monthly summary of the mean, standard deviation (sd), median, minimum (Min), and maximum (Max) concentrations of 6-h meteorological parameters (T (temperature), P (pressure), RH (relative humidity), WS (wind speed) and Rainfall) between mid-July 2020 to mid-February 2021. Only the month with a number of records up to 10 valid days was used. N stands for the number of total datasets used; Supplementary References.

Author Contributions: Conceptualization, methodology, formal analysis, investigation, data curation, writing—original draft preparation, visualization, Y.B., B.E.G. and A.B.; writing—review and editing, A.B. and F.C.; resources, all authors; supervision, A.B. and E.K.E.H.; project administration, A.B., M.T. and F.C. All authors have read and agreed to the published version of the manuscript.

Funding: This research was funded by the bilateral CNRST (Morocco)-CNR (Italy) cooperation framework (Research Contract No 7/2020 PICS Italy).

Institutional Review Board Statement: Not applicable.

Informed Consent Statement: Not applicable.

Data Availability Statement: The datasets generated and analyzed during the current study are not publicly available but are available from the corresponding author upon reasonable request.

Acknowledgments: The authors gratefully acknowledge the NOAA Air Resources Laboratory (ARL) for the provision of the HYSPLIT transport and dispersion model used in this publication.

Conflicts of Interest: The authors declare no conflict of interest.

References

1. Arif, M.; Kumar, R.; Kumar, R.; Eric, Z.; Gourav, P. Ambient Black Carbon, PM_{2.5} and PM₁₀ at Patna: Influence of Anthropogenic Emissions and Brick Kilns. *Sci. Total Environ.* **2018**, *624*, 1387–1400. [[CrossRef](#)] [[PubMed](#)]
2. Manisalidis, I.; Stavropoulou, E.; Stavropoulos, A.; Bezirtzoglou, E. Environmental and Health Impacts of Air Pollution: A Review. *Front. Public Health* **2020**, *8*, 14. [[CrossRef](#)] [[PubMed](#)]
3. Genga, A.; Ielpo, P.; Siciliano, T.; Siciliano, M. Carbonaceous Particles and Aerosol Mass Closure in PM_{2.5} Collected in a Port City. *Atmos. Res.* **2017**, *183*, 245–254. [[CrossRef](#)]
4. WHO. *WHO Global Air Quality Guidelines*; WHO: Geneva, Switzerland, 2021; ISBN 9789812837134.
5. Bounakhla, Y.; Benchrif, A.; Tahri, M.; Costabile, F.; Zahry, F.; Bounakhla, M.; El Hassan, E.K. Black Carbon Aerosols at an Urban Site in North Africa (Kenitra, Morocco). *Atmos. Pollut. Res.* **2022**, *13*, 101489. [[CrossRef](#)]
6. Benchrif, A.; Guinot, B.; Bounakhla, M.; Cachier, H.; Damnati, B.; Baghdad, B. Aerosols in Northern Morocco: Input Pathways and Their Chemical Fingerprint. *Atmos. Environ.* **2018**, *174*, 140–147. [[CrossRef](#)]
7. Otmani, A.; Benchrif, A.; Lachhab, A.; Tahri, M.; Baghdad, B.; El Bouch, M.; Chakir, E.M. Source Apportionment and Diurnal Variability of Autumn-Time Black Carbon in a Coastal City of Salé, Morocco. *Environ. Sci.* **2022**, *19*, 8. [[CrossRef](#)]
8. Blanco-Becerra, L.C.; Gáfarro-Rojas, A.I.; Rojas-Roa, N.Y. Influence of Precipitation Scavenging on the PM_{2.5}/PM₁₀ Ratio at the Kennedy Locality of Bogotá, Colombia. *Rev. Fac. Ing.* **2015**, *2015*, 58–65. [[CrossRef](#)]
9. Danek, T.; Weglinska, E.; Zareba, M. The Influence of Meteorological Factors and Terrain on Air Pollution Concentration and Migration: A Geostatistical Case Study from Krakow, Poland. *Sci. Rep.* **2022**, *12*, 11050. [[CrossRef](#)]
10. Sugimoto, N.; Shimizu, A.; Matsui, I.; Nishikawa, M. A Method for Estimating the Fraction of Mineral Dust in Particulate Matter Using PM_{2.5}-to-PM₁₀ Ratios. *Particuology* **2016**, *28*, 114–120. [[CrossRef](#)]
11. Xu, G.; Jiao, L.; Zhang, B.; Zhao, S.; Yuan, M.; Gu, Y.; Liu, J.; Tang, X. Spatial and Temporal Variability of the PM_{2.5}/PM₁₀ Ratio in Wuhan, Central China. *Aerosol Air Qual. Res.* **2017**, *17*, 741–751. [[CrossRef](#)]
12. Wang, S.; Gao, J.; Guo, L.; Nie, X.; Xiao, X. Meteorological Influences on Spatiotemporal Variation of PM_{2.5} Concentrations in Atmospheric Pollution Transmission Channel Cities of the Beijing–Tianjin–Hebei Region, China. *Int. J. Environ. Res. Public Health* **2022**, *19*, 1607. [[CrossRef](#)] [[PubMed](#)]
13. Gidhagen, L.; Krecl, P.; Targino, A.C.; Polezer, G.; Godoi, R.H.M.; Felix, E.; Cipoli, Y.A.; Charres, I.; Malucelli, F.; Wolf, A.; et al. An Integrated Assessment of the Impacts of PM_{2.5} and Black Carbon Particles on the Air Quality of a Large Brazilian City. *Air Qual. Atmos. Health* **2021**, *14*, 1455–1473. [[CrossRef](#)]
14. EEA. EMEP/EEA Air Pollutant Emission Inventory Guidebook 2016—Update July 2017 1. *Dk* **2015**, *53*, 1689–1699.
15. Zhang, R.; Tao, J.; Ho, K.F.; Shen, Z.; Wang, G.; Cao, J.; Liu, S.; Zhang, L.; Lee, S.C. Characterization of Atmospheric Organic and Elemental Carbon of PM_{2.5} in a Typical Semi-Arid Area of Northeastern China. *Aerosol Air Qual. Res.* **2012**, *12*, 792–802. [[CrossRef](#)]
16. Liu, B.; He, M.M.; Wu, C.; Li, J.; Li, Y.; Lau, N.T.; Yu, J.Z.; Lau, A.K.H.; Fung, J.C.H.; Hoi, K.I.; et al. Potential Exposure to Fine Particulate Matter (PM_{2.5}) and Black Carbon on Jogging Trails in Macau. *Atmos. Environ.* **2019**, *198*, 23–33. [[CrossRef](#)]
17. Yu, N.; Zhu, Y.; Xie, X.; Yan, C.; Zhu, T.; Zheng, M. Characterization of Ultrafine Particles and Other Traffic Related Pollutants near Roadways in Beijing. *Aerosol Air Qual. Res.* **2015**, *15*, 1261–1269. [[CrossRef](#)]
18. Zhao, P.; Dong, F.; Yang, Y.; He, D.; Zhao, X.; Zhang, W.; Yao, Q.; Liu, H. Characteristics of Carbonaceous Aerosol in the Region of Beijing, Tianjin, and Hebei, China. *Atmos. Environ.* **2013**, *71*, 389–398. [[CrossRef](#)]
19. Dotse, S.-Q.; Asane, J.K.; Ofosu, F.G.; Aboh, I.J.K. Particulate Matter and Black Carbon Concentration Levels in Ashaiman, a Semi-Urban Area of Ghana, 2008. *Res. J. Environ. Earth Sci.* **2012**, *4*, 20–25.
20. Mkoma, S.L.; Chi, X.; Maenhaut, W. Characteristics of Carbonaceous Aerosols in Ambient PM₁₀ and PM_{2.5} Particles in Dar Es Salaam, Tanzania. *Sci. Total Environ.* **2010**, *408*, 1308–1314. [[CrossRef](#)]

21. Tahri, M.; Benchrif, A.; Bounakhla, M.; Benyaich, F.; Noack, Y. Seasonal Variation and Risk Assessment of PM_{2.5} and PM_{2.5–10} in the Ambient Air of Kenitra, Morocco. *Environ. Sci. Process. Impacts* **2017**, *19*, 1427–1436. [[CrossRef](#)]
22. Ryś, A.; Samek, L. Measurement Report: Determination of Black Carbon Concentration in PM_{2.5} Fraction by Multi-Wavelength Absorption Black Carbon Instrument (MABI). *Atmos. Chem. Phys. Discuss.* **2021**, *2021*, 1–14.
23. Manohar, M.; Atanacio, A.; Button, D.; Cohen, D. MABI-A Multi-Wavelength Absorption Black Carbon Instrument for the Measurement of Fine Light Absorbing Carbon Particles. *Atmos. Pollut. Res.* **2021**, *12*, 133–140. [[CrossRef](#)]
24. NOAA Accessing Data Selection Screen for Surface Data Hourly Global (DS3505). Available online: <https://www7.ncdc.noaa.gov/CDO/cdo> (accessed on 1 March 2022).
25. Carslaw, D. Worldmet: Import Surface Meteorological Data from NOAA Integrated Surface Database (ISD). R Package version 0.9.5. 2021. Available online: <https://CRAN.R-project.org/package=worldmet> (accessed on 1 March 2022).
26. Hsu, Y.K.; Holsen, T.M.; Hopke, P.K. Comparison of Hybrid Receptor Models to Locate PCB Sources in Chicago. *Atmos. Environ.* **2003**, *37*, 545–562. [[CrossRef](#)]
27. Draxler, R.R.; Rolph, G.D. HYSPLIT (HYbrid Single-Particle Lagrangian Integrated Trajectory) Model Access via NOAA ARL READY Website. NOAA Air Resources Laboratory, College Park, MD. 2014; Volume 8. Available online: <http://www.arl.noaa.gov/HYSPLIT.php> (accessed on 1 March 2022).
28. Rolph, G.; Stein, A.; Stunder, B. Real-Time Environmental Applications and Display System: READY. *Environ. Model. Softw.* **2017**, *95*, 210–228. [[CrossRef](#)]
29. Petit, J.E.; Favez, O.; Albinet, A.; Canonaco, F. A User-Friendly Tool for Comprehensive Evaluation of the Geographical Origins of Atmospheric Pollution: Wind and Trajectory Analyses. *Environ. Model. Softw.* **2017**, *88*, 183–187. [[CrossRef](#)]
30. Ferenczi, Z.; Imre, K.; Lakatos, M.; Molnár, Á.; Bozó, L.; Homolya, E.; Gelencsér, A. Long-Term Characterization of Urban PM₁₀ in Hungary. *Aerosol Air Qual. Res.* **2021**, *21*, 210048. [[CrossRef](#)]
31. Luo, H.; Zhou, W.; Jiskani, I.M.; Wang, Z. Analyzing Characteristics of Particulate Matter Pollution in Open-Pit Coal Mines: Implications for Green Mining. *Energies* **2021**, *14*, 2680. [[CrossRef](#)]
32. Hebbali, A. Tools for Building OLS Regression Models. R package olsrr version 0.5.3. 2020. Available online: <https://CRAN.R-project.org/package=olsrr> (accessed on 1 March 2022).
33. Akaike, H. A New Look at the Statistical Model Identification. *IEEE Trans. Automat. Contr.* **1974**, *19*, 716–723. [[CrossRef](#)]
34. Schwarz, G. 1978 Schwarz. *Ann. Stat.* **1978**, *6*, 461–464.
35. Akaike, H. On Newer Statistical Approaches to Parameter Estimation and Structure Determination. *IFAC Proc. Vol.* **1978**, *11*, 1877–1884. [[CrossRef](#)]
36. Mallows, C.L. Some Comments on Cp. *Technometrics* **1973**, *15*, 661–675. [[CrossRef](#)]
37. R Development Core Team R Core Team (2020). R: A Language and Environment for Statistical Computing. R Foundation for Statistical Computing, Vienna, Austria. *R Found. Stat. Comput.* **2019**, *2*. Available online: <https://www.R-Project.Org/> (accessed on 1 March 2021).
38. Carslaw, D.C.; Ropkins, K. Openair-An R Package for Air Quality Data Analysis. *Environ. Model. Softw.* **2012**, *27–28*, 52–61. [[CrossRef](#)]
39. Lin, X.; Chen, J.; Lu, T.; Huang, D.; Zhang, J. Air Pollution Characteristics and Meteorological Correlates in Lin'an, Hangzhou, China. *Aerosol Air Qual. Res.* **2019**, *19*, 2770–2780. [[CrossRef](#)]
40. Ait Bouh, H.; Benyaich, F.; Bounakhla, M.; Noack, Y.; Tahri, M.; Zahry, F. Seasonal Variations of the Atmospheric Particles and Its Chemical Components in Meknes City Morocco. *J. Mater. Environ. Sci.* **2013**, *4*, 49–62.
41. Pérez, N.; Pey, J.; Cusack, M.; Reche, C.; Querol, X.; Alastuey, A.; Viana, M. Variability of Particle Number, Black Carbon, and PM₁₀, PM_{2.5}, and PM₁ Levels and Speciation: Influence of Road Traffic Emissions on Urban Air Quality. *Aerosol Sci. Technol.* **2010**, *44*, 487–499. [[CrossRef](#)]
42. Hueglin, C.; Buchmann, B.; Weber, R.O. Long-Term Observation of Real-World Road Traffic Emission Factors on a Motorway in Switzerland. *Atmos. Environ.* **2006**, *40*, 3696–3709. [[CrossRef](#)]
43. Begum, B.A.; Saroar, G.; Nasiruddin, M.; Randal, S.; Sivertsen, B.; Hopke, P.K. Particulate Matter and Black Carbon Monitoring at Urban Environment in Bangladesh. *Nucl. Sci. Appl.* **2014**, *23*, 1–8.
44. Şahin, Ü.A.; Onat, B.; Akin, Ö.; Ayvaz, C.; Uzun, B.; Mangır, N.; Doğan, M.; Harrison, R.M. Temporal Variations of Atmospheric Black Carbon and Its Relation to Other Pollutants and Meteorological Factors at an Urban Traffic Site in Istanbul. *Atmos. Pollut. Res.* **2020**, *11*, 1051–1062. [[CrossRef](#)]
45. Abuelgasim, A.; Farahat, A. Investigations on PM₁₀, PM_{2.5}, and Their Ratio over the Emirate of Abu Dhabi, United Arab Emirates. *Earth Syst. Environ.* **2020**, *4*, 763–775. [[CrossRef](#)]
46. Zghaid, M.; Noack, Y.; Bounakla, M.; Benyaich, F. Pollution Atmosphérique Particulaire Dans La Ville de Kenitra (Maroc). *Pollut. Atmos.* **2009**, *51*, 313–324. [[CrossRef](#)]
47. Rajeevan, K.; Sumesh, R.K.; Resmi, E.A.; Unnikrishnan, C.K. An Observational Study on the Variation of Black Carbon Aerosol and Source Identification over a Tropical Station in South India. *Atmos. Pollut. Res.* **2019**, *10*, 30–44. [[CrossRef](#)]
48. Hang, N.T.; Kim Oanh, N.T. Chemical Characterization and Sources Apportionment of Fine Particulate Pollution in a Mining Town of Vietnam. *Atmos. Res.* **2014**, *145–146*, 214–225. [[CrossRef](#)]
49. Zhang, X.; Li, Z.; Wang, F.; Song, M.; Zhou, X.; Ming, J. Carbonaceous Aerosols in PM₁, PM_{2.5}, and PM₁₀ Size Fractions over the Lanzhou City, Northwest China. *Atmosphere* **2020**, *11*, 1368. [[CrossRef](#)]

50. Quiros, D.C.; Zhang, Q.; Choi, W.; He, M.; Paulson, S.E.; Winer, A.M.; Wang, R.; Zhu, Y. Air Quality Impacts of a Scheduled 36-h Closure of a Major Highway. *Atmos. Environ.* **2013**, *67*, 404–414. [[CrossRef](#)]
51. Viidanoja, J.; Sillanpää, M.; Laakia, J.; Kerminen, V.M.; Hillamo, R.; Aarnio, P.; Koskentalo, T. Organic and Black Carbon in PM_{2.5} and PM₁₀: 1 Year of Data from an Urban Site in Helsinki, Finland. *Atmos. Environ.* **2002**, *36*, 3183–3193. [[CrossRef](#)]
52. Czernecki, B.; Pórolniczak, M.; Kolendowicz, L.; Marosz, M.; Kendzierski, S.; Pilgij, N. Influence of the Atmospheric Conditions on PM₁₀ Concentrations in Poznań, Poland. *J. Atmos. Chem.* **2017**, *74*, 115–139. [[CrossRef](#)]
53. Kliengchuay, W.; Worakhunpiset, S.; Limpanont, Y.; Meeyai, A.C.; Tantrakarnapa, K. Influence of the Meteorological Conditions and Some Pollutants on PM₁₀ Concentrations in Lamphun, Thailand. *J. Environ. Health Sci. Eng.* **2021**, *19*, 237–249. [[CrossRef](#)]
54. Krampah, F.; Amegbey, N.; Ndur, S. Spatio-Temporal Distribution and Health Risk Levels of TSP and PM₁₀ in the Mining Town of Tarkwa, Ghana. *Ghana Min. J.* **2021**, *21*, 53–67. [[CrossRef](#)]
55. Chen, T.; He, J.; Lu, X.; She, J.; Guan, Z. Spatial and Temporal Variations of PM_{2.5} and Its Relation to Meteorological Factors in the Urban Area of Nanjing, China. *Int. J. Environ. Res. Public Health* **2016**, *13*, 921. [[CrossRef](#)] [[PubMed](#)]
56. Yang, Q.; Yuan, Q.; Li, T.; Shen, H.; Zhang, L. The Relationships between PM_{2.5} and Meteorological Factors in China: Seasonal and Regional Variations. *Int. J. Environ. Res. Public Health* **2017**, *14*, 1510. [[CrossRef](#)]
57. Guo, L.C.; Zhang, Y.; Lin, H.; Zeng, W.; Liu, T.; Xiao, J.; Rutherford, S.; You, J.; Ma, W. The Washout Effects of Rainfall on Atmospheric Particulate Pollution in Two Chinese Cities. *Environ. Pollut.* **2016**, *215*, 195–202. [[CrossRef](#)] [[PubMed](#)]
58. Yang, Z.; Yang, J.; Li, M.; Chen, J.; Ou, C.Q. Nonlinear and Lagged Meteorological Effects on Daily Levels of Ambient PM_{2.5} and O₃: Evidence from 284 Chinese Cities. *J. Clean. Prod.* **2021**, *278*, 123931. [[CrossRef](#)]
59. Ito, K.; Thurston, G.D.; Silverman, R.A. Characterization of PM_{2.5}, Gaseous Pollutants, and Meteorological Interactions in the Context of Time-Series Health Effects Models. *J. Expo. Sci. Environ. Epidemiol.* **2007**, *17*, S45–S60. [[CrossRef](#)] [[PubMed](#)]
60. Huang, F.; Li, X.; Wang, C.; Xu, Q.; Wang, W.; Luo, Y.; Tao, L.; Gao, Q.; Guo, J.; Chen, S.; et al. PM_{2.5} Spatiotemporal Variations and the Relationship with Meteorological Factors during 2013–2014 in Beijing, China. *PLoS ONE* **2015**, *10*, e0141642. [[CrossRef](#)] [[PubMed](#)]
61. Munir, S.; Habeebullah, T.M.; Mohammed, A.M.F.; Morsy, E.A.; Rehan, M.; Ali, K. Analysing PM_{2.5} and Its Association with PM₁₀ and Meteorology in the Arid Climate of Makkah, Saudi Arabia. *Aerosol Air Qual. Res.* **2017**, *17*, 453–464. [[CrossRef](#)]
62. Barmpadimos, I.; Hueglin, C.; Keller, J.; Henne, S.; Prévôt, A.S.H. Influence of Meteorology on PM₁₀ Trends and Variability in Switzerland from 1991 to 2008. *Atmos. Chem. Phys.* **2011**, *11*, 1813–1835. [[CrossRef](#)]
63. Charron, A.; Harrison, R.M. Primary Particle Formation from Vehicle Emissions during Exhaust Dilution in the Roadside Atmosphere. *Atmos. Environ.* **2003**, *37*, 4109–4119. [[CrossRef](#)]
64. Wang, F.; Li, Z.; Wang, F.; You, X.; Xia, D.; Zhang, X.; Zhou, X. Air Pollution in a Low-Industry City in China’s Silk Road Economic Belt: Characteristics and Potential Sources. *Front. Earth Sci.* **2021**, *9*, 527475. [[CrossRef](#)]
65. Wang, J.; Ogawa, S. Effects of Meteorological Conditions on PM_{2.5} Concentrations in Nagasaki, Japan. *Int. J. Environ. Res. Public Health* **2015**, *12*, 9089–9101. [[CrossRef](#)] [[PubMed](#)]
66. Liu, Z.; Shen, L.; Yan, C.; Du, J.; Li, Y.; Zhao, H. Analysis of the Influence of Precipitation and Wind on PM_{2.5} and PM₁₀ in the Atmosphere. *Adv. Meteorol.* **2020**, *2020*, 5039613. [[CrossRef](#)]
67. Dung, N.A.; Son, D.H.; Hanh, N.T.D.; Tri, D.Q. Effect of Meteorological Factors on PM₁₀ Concentration in Hanoi, Vietnam. *J. Geosci. Environ. Prot.* **2019**, *7*, 138–150. [[CrossRef](#)]
68. Zhang, H.; Wang, Y.; Hu, J.; Ying, Q.; Hu, X.M. Relationships between Meteorological Parameters and Criteria Air Pollutants in Three Megacities in China. *Environ. Res.* **2015**, *140*, 242–254. [[CrossRef](#)] [[PubMed](#)]
69. Tan, Y.; Wang, H.; Shi, S.; Shen, L.; Zhang, C.; Zhu, B.; Guo, S.; Wu, Z.; Song, Z.; Yin, Y.; et al. Annual Variations of Black Carbon over the Yangtze River Delta from 2015 to 2018. *J. Environ. Sci.* **2020**, *96*, 72–84. [[CrossRef](#)]
70. Popovicheva, O.B.; Volpert, E.; Sitnikov, N.M.; Chichayeva, M.A.; Padoan, S. Black Carbon in Spring Aerosols of Moscow Urban Background. *Geogr. Environ. Sustain.* **2020**, *13*, 233–243. [[CrossRef](#)]
71. Huang, Y.; Zhang, L.; Qiu, Y.; Chen, Y.; Shi, G.; Li, T.; Zhang, L.; Yang, F. Five-Year Record of Black Carbon Concentrations in Urban Wanzhou, Sichuan Basin, China. *Aerosol Air Qual. Res.* **2020**, *20*, 1282–1293. [[CrossRef](#)]
72. Chen, X.; Zhang, Z.; Engling, G.; Zhang, R.; Tao, J.; Lin, M.; Sang, X.; Chan, C.; Li, S.; Li, Y. Characterization of Fine Particulate Black Carbon in Guangzhou, a Megacity of South China. *Atmos. Pollut. Res.* **2014**, *5*, 361–370. [[CrossRef](#)]
73. Wang, Y.; Wang, X.; Kondo, Y.; Kajino, M.; Munger, J.W.; Hao, J. Black Carbon and Its Correlation with Trace Gases at a Rural Site in Beijing: Top-down Constraints from Ambient Measurements on Bottom-up Emissions. *J. Geophys. Res. Atmos.* **2011**, *116*, D24304. [[CrossRef](#)]
74. Fossum, K.N.; Ovadnevaite, J.; Liu, D.; Flynn, M.; O’Dowd, C.; Ceburnis, D. Background Levels of Black Carbon over Remote Marine Locations. *Atmos. Res.* **2022**, *271*, 106119. [[CrossRef](#)]
75. Cesari, D.; Merico, E.; Dinoi, A.; Marinoni, A.; Bonasoni, P.; Contini, D. *Seasonal Variability of Carbonaceous Aerosols in an Urban Background Area in Southern Italy*; Elsevier: Amsterdam, The Netherlands, 2018; Volume 200, ISBN 3908322987.
76. Barman, N.; Gokhale, S. Urban Black Carbon-Source Apportionment, Emissions and Long-Range Transport over the Brahmaputra River Valley. *Sci. Total Environ.* **2019**, *693*, 133577. [[CrossRef](#)] [[PubMed](#)]
77. Wang, F.; Zhang, X.; Yue, X.; Song, M.; Zhang, G.; Ming, J. Black Carbon: The Concentration and Sources Study at the Nam Co Lake, the Tibetan Plateau from 2015 to 2016. *Atmosphere* **2020**, *11*, 624. [[CrossRef](#)]

78. Oguntoke, O.; Ojelede, M.E.; Annegarn, H.J. Frequency of Mine Dust Episodes and the Influence of Meteorological Parameters on the Witwatersrand Area, South Africa. *Int. J. Atmos. Sci.* **2013**, *2013*, 128463. [[CrossRef](#)]
79. Bibi, S.; Alam, K.; Chishtie, F.; Bibi, H.; Rahman, S. Temporal Variation of Black Carbon Concentration Using Aethalometer Observations and Its Relationships with Meteorological Variables in Karachi, Pakistan. *J. Atmos. Sol. -Terr. Phys.* **2017**, *157–158*, 67–77. [[CrossRef](#)]
80. Grange, S.K.; Lewis, A.C.; Carslaw, D.C. Source Apportionment Advances Using Polar Plots of Bivariate Correlation and Regression Statistics. *Atmos. Environ.* **2016**, *145*, 128–134. [[CrossRef](#)]

Disclaimer/Publisher's Note: The statements, opinions and data contained in all publications are solely those of the individual author(s) and contributor(s) and not of MDPI and/or the editor(s). MDPI and/or the editor(s) disclaim responsibility for any injury to people or property resulting from any ideas, methods, instructions or products referred to in the content.